Pavel A. Perezhogin*, Andrey V. Glazunov, Evgeny V. Mortikov, and Valentin P. Dymnikov

Comparison of numerical advection schemes in two-dimensional turbulence simulation

Abstract: The influence of numerical approximations on statistical characteristics of modelled two-dimensional turbulence sustained by a stochastic external forcing is studied. The ability of various finite-difference and semi-Lagrangian schemes to reproduce reliably the dual energy and enstrophy cascades for coarse spatial resolution is tested. It is also studied how the requirement of preserving invariants inherent to a two-dimensional ideal fluid is important relative to numerical schemes. The results of calculations with high spatial resolution were taken as a reference solution. The choice of studied schemes was motivated by their use in atmosphere and ocean numerical models, in particular, in the Institute of Numerical Mathematics climate model (INMCM) and semi-Lagrangian absolute vorticity (SLAV) model of medium-range weather forecast. The importance of conservation laws for integral vorticity and enstrophy is revealed in the numerical experiments with a small-scale external forcing.

Keywords: Two-dimensional turbulence, numerical schemes, conservation laws.

MSC 2010: 76F05, 76F65, 76M20, 76M12

DOI: 10.1515/rnam-2017-0005
Received July 5, 2016; accepted November 30, 2016

1 Introduction

The dynamics of a two-dimensional ideal incompressible fluid is described by the following equation

$$\frac{\partial w}{\partial t} + J(\psi, w) = 0 \tag{1.1}$$

where J is the Jacobian, ψ and w are the stream function and vorticity related by the ratio $\triangle\psi = w$. In addition to the conservation law for the momentum $\mathbf{P}$ and energy E, equation (1.1) in a doubly-periodic domain possesses an infinite number of invariants (Casimirs) of the form

$$G = \int \Phi(w)\,\mathrm{d}x\mathrm{d}y = \mathrm{const} \tag{1.2}$$

where Φ is a smooth function. The most simple Casimir invariants are the integral vorticity Ω and the enstrophy Z (the Casimirs obtained with the choice $\Phi(w) = w$ and $\Phi(w) = w^2/2$ in expression (1.2), respectively).

It is assumed that the most important invariants are the enstrophy Z and the energy E determining the mean weighted square of the wave number over the energy [10]:

$$\overline{k^2} = \frac{\int k^2 E(k)\mathrm{d}k}{\int E(k)\mathrm{d}k} = \frac{Z}{E} \tag{1.3}$$

where $E(k)$ is the spectral density of the kinetic energy. The number $\overline{k^2}$ determines the typical scale of the flow. The preservation of the number $\overline{k^2}$ poses strong restrictions on the energy transport over the spectrum.

***Corresponding Author: Pavel A. Perezhogin:** Institute of Numerical Mathematics of the RAS, Moscow 119333, Russia. Moscow Institute of Physics and Technology, Dolgoprudny 141701, Moscow Region, Russia. E-mail: pperezhogin@gmail.com
Andrey V. Glazunov, Valentin P. Dymnikov: Institute of Numerical Mathematics of the RAS, Moscow 119333, Russia. Moscow Institute of Physics and Technology, Dolgoprudny 141701, Moscow Region, Russia
Evgeny V. Mortikov: Scientific Research Computing Center of Lomonosov Moscow State University, Moscow 119234, Russia. Institute of Numerical Mathematics of the RAS, Moscow 119333, Russia

We generalize system (1.1) by adding a forcing F and dissipative terms D. In this case we have

$$\frac{\partial w}{\partial t} + J(\psi, w) = F + D. \tag{1.4}$$

Under the conditions of dynamic chaos, a state of statistical equilibrium is established in such system in the course of time. This state is characterized by mean values over time for some functionals dependent on the solution. The system obtained in this case has no such wide class of invariants as system (1.1) has. The following question naturally arises here: Is it necessary to require fulfillment of conservation laws mentioned above in the asymptotics $F \to 0$ and $D \to 0$ in the case of numerical solution of equations (1.4)? Such formulation of the problem is natural if we suppose that the equilibrium distributions of the energy and enstrophy over the spectrum have inertial intervals where the dissipation and excitation of the corresponding invariants are small. In what follows, speaking on the dynamics of system (1.4), we mean that 'conservation laws' are those of system (1.1). This issue has a certain practical sense because the problem of numerical climate simulation is focused on the study of equilibrium states and geophysical flows are quasi-two-dimensional.

Due to the nonlinear nature of equations, numerical errors can be in any range of scales. We may mention aliasing errors as an example. Even if numerical errors are concentrated in small scales, then, as was indicated in [17], these errors can be transmitted in time over the spectrum into larger scales due to nonlinear interactions. In the case when the time of such transfer is less than the typical time of energy notable processes the distribution of energy over the spectrum may be violated. The presence or absence of 'conservation laws' for the scheme may affect the form of numerical errors and their distribution over scales.

Discrete approximations of equations (1.1) allow us to preserve only a finite number of invariants. For example, the Arakawa scheme [3] being most appropriate from the viewpoint of the number of preserved invariants possesses discrete conservation laws for the energy, enstrophy, integral vorticity, and momentum. However, other numerical methods are also of some interest, in particular, those are semi-Lagrangian schemes [23] for which even the conservation of the first moments (in our case, integral vorticity) is a rather difficult problem.

In this paper we study how the conservation of invariants in numerical schemes may affect the representation of the complex turbulent flow properties. As a model problem we take the problem of simulation of a homogeneous isotropic turbulence excited by an external stochastic forcing with a fixed spatial scale. According to the theory [12] (Kraichnan–Leith–Batchelor (KLB)), the energy of external forcing is transported to large scales, and the enstrophy is transported to small ones. The corresponding inertial spectral ranges are formed if the dissipation is weak in comparison with the nonlinear interactions. The KLB theory predicts the appearance of an equilibrium state and its form. According to the KLB theory, regardless of the type of forcing chosen in a narrow spectral interval near the wave number k_f, the spectrum of the energy must have the form

$$E(k) = C_1 \varepsilon^{2/3} k^{-5/3}, \quad k < k_f \tag{1.5}$$

$$E(k) = C_2 \eta^{2/3} k^{-3}, \quad k > k_f \tag{1.6}$$

where the constant C_1 is approximately evaluated [6] as $C_1 \approx 6$; ε and η are incoming fluxes of energy and enstrophy per surface unit.

Predictions of the theory regarding the inverse energy cascade are confirmed in many numerical experiments [6, 25]. In the range of the direct enstrophy cascade the energy spectrum slope obtained numerically usually differs a lot from the theoretical predictions, in order to achieve a compliance with the KLB theory, one should either increase the spatial resolution (for example, a grid of 32768×32768 nodes was used in [7]), or use specially selected turbulent closures (see [18]). We consider low resolutions of order 360×360, which approximately corresponds to one degree resolution in atmospheric models and so we do not analyze in detail the energy distribution in the direct cascade (in the domain of large wave numbers).

We consider two types of problems depending on the spatial scale of forcing:

1. A small-scale forcing. The typical scale of forcing equals several mesh sizes (4 or 6 depending on the resolution) or 450 kilometers if we draw an analogy with models of atmosphere.

   In this case it is important to check that a proper inverse energy cascade is formed. It should be noted that, according to [6], when using spectral methods, an inverse cascade can exist under conditions when the direct cascade is virtually absent due to low spatial resolution.

2. A large-scale forcing. The forcing is applied on the wavenumber 4 and corresponds to a scale about 10000 km in models of the atmosphere. Such forcing corresponds to an atmospheric cyclogenesis caused by baroclinic instability and large-scale orography. In this case the main interest is in the formation of a proper direct cascade.

Since the main goal of the paper is to obtain recommendations for the development of promising computational cores for climate models of the INM RAS, we study the schemes traditionally used in various models of atmosphere and ocean of the INM RAS [1, 9], the schemes implemented in new versions of the forecast weather model SLAV [22, 24], and also classic Arakawa schemes [3] and semi-Lagrangian schemes including those presented in [28].

2 Equations and parameters of the model

2.1 Equations of the model in velocity–pressure and vorticity–stream function variables

We consider the dynamics of a two-dimensional incompressible fluid in the square $(x, y) \in [0, 2\pi] \times [0, 2\pi]$ with periodic boundary conditions in Cartesian coordinates. In the velocity–pressure variables equation of motion (1.4) can be written in the following form:

$$\frac{\partial \mathbf{u}}{\partial t} + (\mathbf{u} \cdot \nabla)\mathbf{u} = -\nabla p - \nu \triangle^2 \mathbf{u} - \alpha \mathbf{u} + \mathbf{f} \tag{2.1a}$$

$$\nabla \cdot \mathbf{u} = 0. \tag{2.1b}$$

Here $\mathbf{u} = (U, V)$ is the velocity, p is the pressure, $\mathbf{f}$ is the forcing (external force acting on the flow), $\alpha > 0$ is the Rayleigh friction coefficient. The dissipative term acting on small-scale components of the flow is defined as a biharmonic operator with the coefficient $\nu > 0$. This choice is caused by the necessity to separate spatial scales of forcing and dissipation under a coarse spatial resolution. This corresponds to the common practice to dump numerical noise in models of atmosphere and ocean where dissipative terms acting mainly on the short-wave part of the spectrum are often used.

In the vorticity–stream function variables we have the following notation:

$$\frac{\partial w}{\partial t} + (\mathbf{u} \cdot \nabla)w = -\nu \triangle^2 w - \alpha w + f \tag{2.2a}$$

$$\triangle \psi = w \tag{2.2b}$$

where w is the vorticity, ψ is the stream function, f is the forcing.

Variables in equations (2.1) and (2.2) are related by the following equalities

$$\mathbf{u} = \Big(-\frac{\partial \psi}{\partial y}, \frac{\partial \psi}{\partial x} \Big) \tag{2.3}$$

$$w = \frac{\partial V}{\partial x} - \frac{\partial U}{\partial y}. \tag{2.4}$$

The approximation of equations (2.1), (2.2) uses uniform spatial grid with the mesh sizes (h_x, h_y) and time step τ. We define the difference operators as follows

$$\delta_{x_i} \varphi = \frac{\varphi(x_i + h_{x_i}/2) - \varphi(x_i - h_{x_i}/2)}{h_{x_i}} \tag{2.5}$$

$$\overline{\varphi}^{x_i} = \frac{\varphi(x_i + h_{x_i}/2) + \varphi(x_i - h_{xi}/2)}{2} \tag{2.6}$$

$$\nabla_h \cdot \mathbf{u} = \delta_x U + \delta_y V \tag{2.7}$$

$$\triangle_h \varphi = \nabla_h^2 \varphi = \delta_x(\delta_x \varphi) + \delta_y(\delta_y \varphi). \tag{2.8}$$

2.2 External forcing

The forcing has different form depending on chosen variables. In the variables $(\mathbf{u}, p)$ it is given as

$$\mathbf{f} = \begin{bmatrix} A_f \\ B_f \end{bmatrix} \sin(k_x x + k_y y + \varphi) \tag{2.9}$$

and in the variables (ψ, w) it is calculated by the formula

$$f = C_f \sin(k_x x + k_y y + \varphi). \tag{2.10}$$

Here $\varphi \in [0, 2\pi]$ is a random phase; the wave vector $\mathbf{k} = (k_x, k_y)$ lies in the narrow shell near the wave number k_f, i.e., $\|\mathbf{k}\|_2 \in [k_f - k_\delta/2, k_f + k_\delta/2]$. The numbers k_x, k_y are taken integer and the typical width k_δ of the shell equals 4. The forcing is uncorrelated in time, i.e., (φ, k_x, k_y) are pseudo-random variables.

In the case of natural variables $(\mathbf{u}, p)$, the amplitudes A_f and B_f are taken to provide the divergence-free property for the forcing in its spatial approximation, i.e.,

$$\nabla_h \cdot \mathbf{f}_h = 0 \tag{2.11}$$

where $\mathbf{f}_h$ is the discrete analogue of the forcing and ∇_h is finite difference gradient operator (2.7).

As shown in [2], the influx of energy ε for equations written in form (2.1) depends on the time step and is calculated as

$$\varepsilon = \frac{\tau}{4}(A_f^2 + B_f^2). \tag{2.12}$$

All finite difference schemes in this paper are constructed on the same staggered C-grid (in the terminology of Arakawa) and have the same (second) order of spatial approximation. Specifying the desirable energy influx ε and time step τ, we can calculate the coefficients A_f, B_f from equations (2.12) and (2.11), and the coefficient C_f is obtained from the discrete relation between the vorticity and velocity on the C-grid.

The influxes of enstrophy and energy depend on the relation between difference analogues of these invariants. Semi-Lagrangian schemes in the variables (ψ, w) are implemented on an A-grid and to provide the same relations between difference analogues of the energy and enstrophy as this is on a C-grid the procedure of reconstruction of the velocity $\mathbf{u}$ according to formula (2.3) is performed by application of the Fourier transform with the use of modified wave numbers corresponding to the C-grid. As a result of such approach, numerical experiments with all schemes were performed for external forcing providing the same influxes of energy and enstrophy.

2.3 Dissipative terms

The coefficient at the biharmonic operator ν is taken from the condition of equality of enstrophy influx from the external forcing η and its small-scale dissipation η_ν:

$$\eta_\nu = \eta. \tag{2.13}$$

The original idea of such approach belongs to Lilly [13] for the case of three-dimensional turbulence and turbulence closure of Smagorinsky. The approach presented below is more close to ideas of [5]. However, none of those papers took into account the difference form of the dissipative operator, but the consideration of such operator leads to the considerable correction of the coefficient ν.

It is known that, according to the KLB theory [12], the spectral density of energy has form (1.6) on the direct enstrophy cascade, and the approximate value of the constant $C_2 \approx 1.5$ can be calculated from numerical experiments with high resolution. If we know the form of the energy spectrum and dissipative operators, we can calculate η_ν. For the sake of simplicity, let us consider the action of the difference biharmonic operator onto the function $w = \exp(ikx)$ of one variable, i.e.,

$$\triangle_h^2 w = k'^4 w$$

where $k' = \sin(kh_x/2)/(h_x/2)$ is the modified wave number and $\triangle_h$ is the difference analogue of Laplace operator (2.8).

The contribution of the biharmonic operator to equation of dynamics (2.2) written in the Fourier space has the form

$$\frac{\partial w(k)}{\partial t} = -\nu k'^4 w(k) \tag{2.14}$$

where $w(k)$ is the Fourier transform of the function w. Multiplying (2.14) by $w^*(k)$ ('$*$' is the symbol of complex conjugation) and integrating over the circumference S of radius k in the Fourier space, we obtain the following equation for the balance of enstrophy:

$$\frac{\partial Z(k)}{\partial t} = -2\nu k'^4 Z(k) \tag{2.15}$$

where $Z(k) = \frac{1}{2}\oint_S w(k)w^*(k)$ is the spectral enstrophy density. If we know the relation between the energy and enstrophy

$$Z(k) = k'^2 E(k)$$

which is valid for a C-grid, we can calculate the dissipation of enstrophy by balance formula (2.15) and form (1.6) of the spectral density $E(k)$:

$$\eta_\nu = \int_{k_f}^{k_{\max}} \frac{\partial Z(k)}{\partial t}\mathrm{d}k = -2\nu C_2 \eta^{2/3} \int_{k_f}^{k_{\max}} k^{-3}k'^6 \mathrm{d}k. \tag{2.16}$$

For sufficiently large scales of forcing k_f (with the wavelength not less than three steps of the grid), the integral can be approximated with a good accuracy by the approximate expression

$$\int_{k_f}^{k_{\max}} k^{-3}k'^6 \mathrm{d}k \approx 0.16 \int_{k_f}^{k_{\max}} k^3 \mathrm{d}k = 0.16(k_{\max}^4 - k_f^4)/4.$$

Equating dissipation (2.16) and the influx of enstrophy η, we can calculate the dissipation parameter

$$\nu = 8.32 \frac{\eta^{1/3}}{k_{\max}^4 - k_f^4}. \tag{2.17}$$

Taking into account the form of the biharmonic operator and the difference relation between the enstrophy and energy, we can increase the coefficient ν approximately $1/0.16 \approx 6$ times. Formula (2.17) gives a good estimate in the case when the direct cascade of enstrophy has the sufficient length and slope (-3) close to the KLB theory. If the enstrophy interval is short, then the coefficient should be decreased for empirical reasons.

The coefficient ν is taken the same for schemes in the variables $(\mathbf{u}, p)$ and (w, ψ), and biharmonic operators are equivalent from the viewpoint of the dissipation of enstrophy and energy due to the choice of the same C-grid for all finite difference methods and the use of Fourier transform for semi-Lagrangian methods in the variables (w, ψ) (as was described in Section 2.2).

The coefficient of Rayleigh friction is taken so that the inverse cascade of energy has sufficiently large extent.

3 Numerical methods

3.1 Finite difference schemes in the variables $(\mathbf{u}, p)$

System of equations (2.1) is solved by projection method [8]. The intermediate value $\mathbf{u}'$ is obtained from the following scheme:

$$\frac{\mathbf{u}'_h - \mathbf{u}^n_h}{\tau} = -[(\mathbf{u}\cdot\nabla)\mathbf{u}]^{n+1/2}_h - \nabla_h p^n_h - \nu[\triangle^2_h \mathbf{u}_h]^{n+1/2} - \alpha\mathbf{u}^{n+1/2}_h + \mathbf{f}_h$$

where the values $[(\mathbf{u}\cdot\nabla)\mathbf{u}]_h^{n+1/2}$, $\nu[\triangle^2\mathbf{u}]_h^{n+1/2}$, $\alpha\mathbf{u}_h^{n+1/2}$ are calculated on the $(n+1/2)$th time layer by the second order Adams–Bashforth scheme

$$\varphi^{n+1/2}=\frac{3}{2}\varphi^n-\frac{1}{2}\varphi^{n-1}.$$

The form of the scheme in time does not affect the results of our work because we use small time step (CFL < 0.15); the INMCM model [1] uses the leapfrog scheme of the second order of approximation. The spatial discretization of the advection term $(\mathbf{u}\cdot\nabla)\mathbf{u}$ is denoted by the index h and is changed from a scheme to scheme.

After that we implement the projection onto the subspace of divergence-free fields, i.e.,

$$\mathbf{u}_h^{n+1}=\mathbf{u}_h'-\tau\nabla_h\varphi_h^{n+1}$$

and recalculate the pressure

$$p_h^{n+1}=p_h^n+\varphi_h^{n+1}$$

where φ_h^{n+1} is chosen from the condition

$$\triangle_h\varphi_h^{n+1}=\frac{\nabla_h\cdot\mathbf{u}_h'}{\tau}.$$

3.1.1 Scheme used in the INMOM ocean model

The INMOM model [9] uses the scheme from [15] preserving the energy and implemented with the use of central difference approximation on a staggered C-grid for the term $(\mathbf{u}\cdot\nabla)\mathbf{u}$ written in a skew-symmetric form, i.e.,

$$[(\mathbf{u}\cdot\nabla)U]_h=\frac{1}{2}\left[\overline{\overline{U}^x\delta_xU}^x+\overline{\overline{V}^x\delta_yU}^y\right]+\frac{1}{2}\left[\delta_x(\overline{U}^x\overline{U}^x)+\delta_y(\overline{V}^x\overline{U}^y)\right]$$

$$[(\mathbf{u}\cdot\nabla)V]_h=\frac{1}{2}\left[\overline{\overline{U}^y\delta_xV}^x+\overline{\overline{V}^y\delta_yV}^y\right]+\frac{1}{2}\left[\delta_x(\overline{U}^y\overline{V}^x)+\delta_y(\overline{V}^y\overline{V}^y)\right].$$

3.1.2 Scheme used in the INMCM atmosphere model

The model of the atmosphere included into the INMCM climate model [1] uses one of Arakawa schemes [4]. It preserves the angular momentum on a sphere. It can be obtained from consideration not only the usual coordinate system (x, y), but also the additional system (x', y') obtained on a square grid by counterclockwise rotation by 45 degrees.

The scheme has the following form of a linear combination of the approximations written in two coordinate systems [4]:

$$[(\mathbf{u}\cdot\nabla)U]_h=\frac{2}{3}\left[\overline{\overline{U}^x\delta_xU}^x+\overline{\overline{V}^x\delta_yU}^y\right]+\frac{1}{3}\left[\overline{\overline{U'\delta_{x'}U}^{x'}}+\overline{\overline{V'\delta_{y'}U}^{y'}}\right]$$

$$[(\mathbf{u}\cdot\nabla)V]_h=\frac{2}{3}\left[\overline{\overline{U}^y\delta_xV}^x+\overline{\overline{V}^y\delta_yV}^y\right]+\frac{1}{3}\left[\overline{\overline{U'\delta_{x'}V}^{x'}}+\overline{\overline{V'\delta_{y'}V}^{y'}}\right].$$

3.2 Finite difference schemes in variables (ψ, w)

System of equations (2.2) is solved in two stages. At the first stage we solve evolution equation (2.2a) and obtain the vorticity w^{n+1} on the next time layer by the second order Adams–Bashforth scheme. At the second stage we reconstruct the stream function ψ^{n+1} from the vorticity w^{n+1} according to Poisson equation (2.2b) and using discrete Laplace operator (2.8).

3.2.1 Arakawa schemes

Several schemes possessing various conservation laws were obtained in [3]. They are based on three different forms of advective term in equation (2.2a). It is known that

$$(\mathbf{u}\cdot\nabla)w = J(\psi, w)$$

where J is the Jacobian of the mapping. Function $J(\psi, w)$ can be expressed in three following ways:

$$J_1 = -\frac{\partial\psi}{\partial y}\frac{\partial w}{\partial x} + \frac{\partial\psi}{\partial x}\frac{\partial w}{\partial y} \tag{3.1a}$$

$$J_2 = -\frac{\partial}{\partial x}\Big(\frac{\partial\psi}{\partial y}w\Big) + \frac{\partial}{\partial y}\Big(\frac{\partial\psi}{\partial x}w\Big) \tag{3.1b}$$

$$J_3 = \frac{\partial}{\partial x}\Big(\frac{\partial w}{\partial y}\psi\Big) - \frac{\partial}{\partial y}\Big(\frac{\partial w}{\partial x}\psi\Big). \tag{3.1c}$$

If we mark the central difference approximation of these Jacobians with the index h, then the scheme preserving the enstrophy **Z** takes the form

$$\frac{1}{2}(J_{1_h} + J_{2_h})$$

for the scheme preserving the energy **E** we have

$$\frac{1}{2}(J_{1_h} + J_{3_h})$$

for that preserving the enstrophy and energy **ZE** we have

$$\frac{1}{3}(J_{1_h} + J_{2_h} + J_{3_h})$$

and for the case of absence of quadratic invariants **N** we have

$$J_{1_h}.$$

3.3 Semi-Lagrangian methods in the variables (ψ, w)

System of equations (2.2) is solved in two steps similar to the case of previous Section 3.2. However, the reconstruction of the stream function ψ^{n+1} from the vorticity w^{n+1} is followed by the determination of the velocity $\mathbf{u}^{n+1}$ on the A-grid (as was described in Section 2.2). The following semi-Lagrangian method is used for recalculation of w^{n+1} on the next time layer:

$$\frac{w_A^{n+1} - w_D^n}{\tau} = F(w^n)_A$$

where A are the arrival points of the trajectory positioned at the grid nodes, D are the departure ones. Since the dissipative terms and the external forcing do not require high calculation accuracy, the right-hand side $F(w)$ is approximated in time with the first order of accuracy. The value w_D^n is calculated by interpolation, and the schemes differ from each other only in the form of interpolant. The determination of trajectories is performed by the SETTLS scheme [11] used in the SLAV model [24]. For the characteristic equation

$$\frac{\mathrm{d}\mathbf{x}}{\mathrm{d}t} = \mathbf{u}$$

it has the form

$$\frac{\mathbf{x}_A^{n+1} - \mathbf{x}_D^n}{\tau} = \frac{1}{2}([2\mathbf{u}^n - \mathbf{u}^{n-1}]_D + \mathbf{u}_A^n). \tag{3.2}$$

The scheme is implicit with respect to the point D and is solved iteratively in 5 iterations with the use of cubic interpolation of the velocity at the point D.

3.3.1 Types of interpolation

We differentiate semi-Lagrangian methods in the type of one-dimensional interpolation only. There are many ways to represent a two-dimensional problem of interpolation as a sequence of one-dimensional ones [20, 28]. Among all methods we choose the cascade approach [20] because it is used in the new version of the SLAV model [22]. In addition to the cascade approach, we also tested the method of tensor product [28], and we did not detect any significant differences in our experiments.

We studied the following types of one-dimensional interpolation:

1. *Cubic* Lagrange interpolation [14] (marked as 'cubic' in figures).
2. Cubic *spline* with periodic boundary conditions [26] (marked as 'spline').
3. *Hermite* interpolation (marked as 'hermite'). It satisfies all necessary and sufficient conditions of monotonicity [28] (the monotonicity means the monotonicity of the interpolant on the grid step). We take the monotonicity conditions 'NCM1' and 'SCM' from [28]. To construct the interpolant on a segment, we have to know the values of the function and its derivatives at the segment endpoints. The values of the function are known and the values of the derivative are calculated with the use of cubic interpolant (see 'cubic derivative estimate' in [28]). Further, the values of the derivative are tested for monotonicity. If monotonicity conditions are fulfilled, the interpolation remains cubic, otherwise some correction follows.
4. Cascade finite-volume semi-Lagrangian scheme [16] (marked as CCS). Using the cascade approach, a sequence of one-dimensional redistributions of mass contained in a computation cell is performed in this scheme. Given the one-dimensional conservation law of form

$$\frac{\partial \rho}{\partial t} + \frac{\partial \rho u_x}{\partial x} = 0$$

the redistribution of mass is expressed as

$$\int\limits_{A(t^{n+1})} \rho \mathrm{d}x = \int\limits_{A(t^n)} \rho \mathrm{d}x \tag{3.3}$$

where $A(t)$ is the volume moving with the fluid and coinciding with a computation cell at the time moment t^{n+1}. The integral in the right-hand side of formula (3.3) is calculated approximately with the use of conservative piecewise-parabolic interpolation.

The basic interpolant in the dynamical core of the SLAV model is cubic, it can be switched to a spline interpolation with approximate matrix inversion, and conservative CCS scheme is used for transfer of admixtures [22].

3.4 Semi-Lagrangian methods in the variables ($\mathbf{u}$, p)

System of equations (2.1) is solved by a projection method similar to the approach described in Section 3.1 using semi-Lagrangian methods described in Section 3.3, however, the processing of the pressure is different and has the form of Crank–Nicolson scheme [29]:

$$\frac{\mathbf{u}_A^{n+1} - \mathbf{u}_D^n}{\tau} = -\frac{1}{2}(\nabla_h p_A^{n+1} + \nabla_h p_D^n).$$

4 Numerical experiments

4.1 Small-scale forcing

Equations (2.1), (2.2) are solved by different numerical schemes described in Section 3 on a grid with the resolution 540×540. The maximum wave number in this problem is $k_{\max} = N/2 = 270$ and the minimum

one is $k_{\min} = 1$. The forcing is defined at a spherical shell of thickness $k_\delta = 4$ near the wave number $k_f = 90$, which corresponds to short waves with the wavelength $6h$. The forcing is uncorrelated in time and provides the energy influx $\varepsilon = 1.534 \cdot 10^{-4}$ in average per surface unit. The Rayleigh friction coefficient is $\alpha = 0.012$ and the coefficient at the biharmonic operator is calculated by formula (2.17) (but then is decreased 4 times because the enstrophy interval is short), i.e., $\nu = 4.26 \cdot 10^{-10}$. In order to indicate typical features of the schemes, we increase or decrease the original resolution of the problem; in this case all parameters of the problem remain as before except for the coefficient at the biharmonic operator which varies according to formula (2.17) (the coefficient decreases 4 times).

The equations are solved until the time moment $t = 100$ (approximately 4000 steps in time for semi-Lagrangian schemes) to reach the state of statistical equilibrium, and after that the calculations for next 500 time units are performed to obtain averaged values of parameters using for this averaging each tenth time step. The Courant number (CFL) was taken equal to 1 for semi-Lagrangian systems because it is optimal from different points of view. As a rule, semi-Lagrangian methods are not used for small CFL, on the other hand, the choice CFL > 1 can lead to the violation of stability condition due to the intersection of the Lagrangian trajectories. Finite difference schemes are calculated for CFL $= 0.15$. The Courant number is obtained taking into account the maximal velocity in the high resolution model (HRM). This model is calculated with the use of ZE scheme on a more fine grid of 2016×2016 nodes and serves as a reference solution.

The inverse energy cascade is responsible for the level of energy in the system. This cascade forms an energy flow to large scales where it is dissipated by Rayleigh friction, and hence we can express the energy level in the following simple form:

$$E = \frac{\varepsilon}{2\alpha}. \tag{4.1}$$

The reference HRM solution suits well relation (4.1), but for the resolution of 540×540 it is worse because of scheme effects.

4.1.1 Finite difference schemes

The equilibrium occurs in the system because of the balance between the influx of forcing and dissipation caused by scheme effects, the biharmonic filter, and Rayleigh friction. The averaged values of the fluxes caused by these three factors and the levels of quadratic invariants are listed in Table 1. The values of levels of invariants are normalized by the corresponding values in HRM. The influxes are normalized by the generation of the forcing. Negative values correspond to dissipation, positive ones to generation. Thus, the sum of values of the cells 'scheme', 'filter', 'friction' equals 100%.

The spectral energy density for the standard resolution of 540×540 and reduced one 360×360 (the wave length of the forcing is equal to $4h$) are shown in Fig. 1. This figure illustrates the process of violation of the inverse cascade for coarse resolutions. As seen from Fig. 1b, independently of the variables involved in notation of equations practically all finite difference schemes have a similar form of spectrum in large scales except for two schemes, namely, E and INMOM, which preserve the energy only. These schemes have sufficiently low level of energy because they generate the enstrophy in small scales where it is dissipated by the numerical filter, which implies the dissipation of energy. A higher generation of enstrophy is observed for the scheme N (139%), however, this does not lead to the differences in energy spectrum in large scales due to the fact that it is accompanied by a considerable artificial generation of energy (36%).

The INMCM scheme has the highest level of energy and it is even higher than for the scheme ZE with two quadratic invariants. This occurs due to two reasons. First, it is practically conservative relative to energy, namely, -0.33%. Second, the enstrophy is dissipated by the scheme, namely, -32%. The dissipation of the enstrophy by the scheme reduces the impact of numerical filter, which, in contrast to the scheme, dissipates the energy together with the enstrophy.

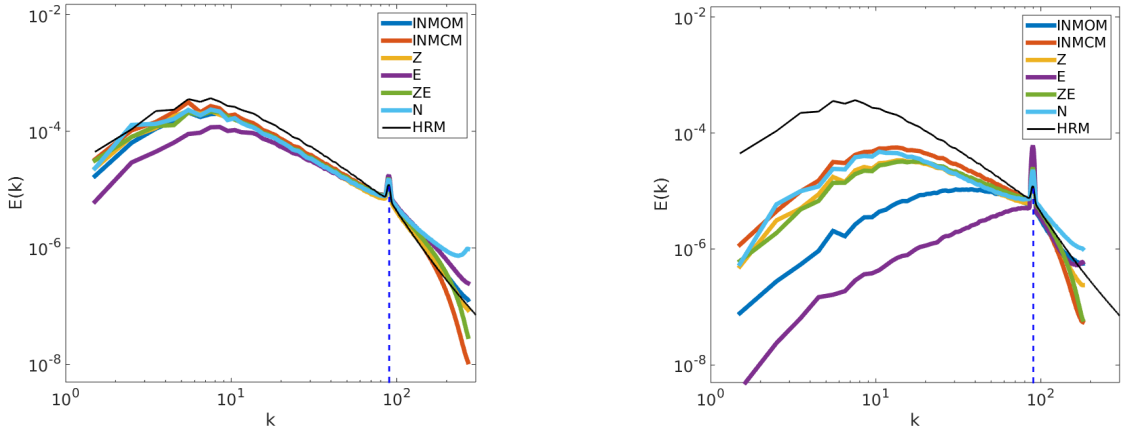

(a) Resolution 540×540.

(b) Resolution 360×360.

Figure 1. Energy spectrum in the logarithmic scale for finite difference schemes in the experiment with small-scale forcing, dotted line indicates the position of forcing.

Table 1. Balance of energy and enstrophy for finite difference schemes in the experiment with small scale forcing, the resolution is 540×540.

Scheme	Energy				Enstrophy			
	level	influx			level	influx		
		scheme	filter	friction		scheme	filter	friction
INMOM	64%	0%	-38%	-62%	71%	23%	-110%	-13%
INMCM	75%	-0,33%	-27%	-72%	67%	-32%	-55%	-12%
Z	64%	-5%	-34%	-62%	66%	0%	-84%	-12%
E	49%	0%	-53%	-47%	86%	61%	-145%	-16%
ZE	66%	0%	-37%	-63%	75%	0%	-87%	-14%
N	68%	36%	-71%	-65%	99%	139%	-221%	-18%
HRM	100%	0%	-4%	-96%	100%	0%	-83%	-17%

4.1.2 Semi-Lagrangian methods

As seen from Fig. 2, CCS interpolants (in the variables (ψ, w)) and spline interpolants (in the variables $(\mathbf{u}, p)$) are the most close to HRM and, according to Table 2, their energy and enstrophy characteristics differ from each other by several percents, which indicates good dissipative properties of the CCS scheme because the spline interpolation is known for its not high dissipative properties. CCS is the only interpolant in the variables (ψ, w) having a proper form of the energy spectrum (energy is not accumulated in large scales). Below we study only three remaining interpolants.

As shown in [27], the semi-Lagrangian method with cubic interpolation and also with interpolants obtained on the base of cubic polynomials (Hermite, spline) is dissipative. This means that we can observe the dissipation of the square of the transported variable. In the case of variables $(\mathbf{u}, p)$ we should expect dissipation of the energy by the scheme and this was confirmed in our experiments. In the case of variables (ψ, w) we may expect only dissipation of the enstrophy, but the energy may be involved in different processes, i.e., generation (Hermite), dissipation (cubic, CCS), and the case close to conservation (spline).

A large number of Hermite interpolants were studied in [27] for the problem of transfer of a passive admixture by a three-dimensional turbulence field. In this case the main difference between interpolants was in the level of dissipation. In our experiments in the variables $(\mathbf{u}, p)$ the difference between interpolants similarly consists in the level of dissipation, which determines the level of energy in the system. The form of energy spectrum is correct here in contrast to semi-Lagrangian methods in the variables (ψ, w).

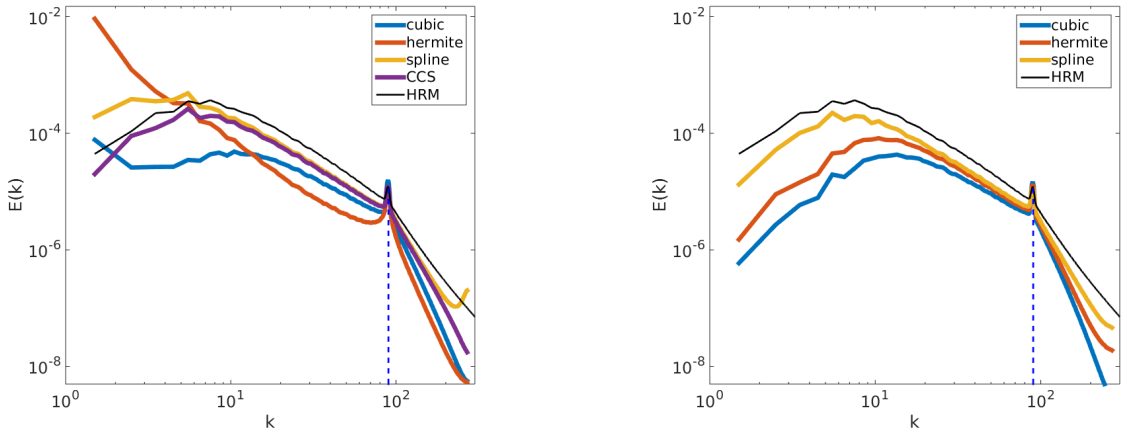

(a) Variables (ψ, w). **(b)** Variables $(\mathbf{u}, p)$.

Figure 2. Energy spectrum in a logarithmic scale for semi-Lagrangian schemes in the experiment with a small-scale forcing, the dotted lines indicates the position of forcing.

Table 2. Balance of energy and enstrophy for semi-Lagrangian schemes in the experiment with a small-scale forcing, resolution 540×540.

	Scheme	Energy				Enstrophy			
		level	influx			level	influx		
			scheme	filter	friction		scheme	filter	friction
(ψ, w)	cubic	26%	-64%	-11%	-25%	32%	-77%	-17%	-6%
	Hermite	211%	110%	-7%	-203%	21%	-85%	-11%	-4%
	spline	85%	3%	-22%	-81%	51%	-38%	-52%	-9%
	CCS	59%	-27%	-17%	-57%	46%	-59%	-33%	-8%
$(\mathbf{u}, p)$	cubic	23%	-68%	-10%	-22%	32%	-80%	-14%	-5%
	Hermite	35%	-53%	-13%	-34%	39%	-69%	-23%	-7%
	spline	58%	-26%	-18%	-56%	48%	-50%	-40%	-8%
	HRM	100%	0%	-4%	-96%	100%	0%	-83%	-17%

Among all schemes presented in the paper, only cubic, Hermite, and spline schemes in the variables (ψ, w) do not preserve the integral vorticity. We can show that all finite difference schemes in the variables (ψ, w) described in this paper preserve it, and all the schemes in the variables $(\mathbf{u}, p)$ preserve an analogue of integral vorticity if we introduce the vorticity at nodes of C-grid by numerical differentiation of the velocity. As seen from Fig. 2, all schemes not possessing the conservation law for the integral vorticity accumulate the energy in large scales, Hermite scheme possesses this property for the resolution increased twice (not shown in the picture). The amount of energy accumulated in large scales is in accordance with the non-conservativity rate of the scheme, it was shown in [27] that the Hermite scheme is the most non-conservative among the schemes presented in the paper. In order to confirm the importance of the integral vorticity conservation, we studied finite difference upwind schemes of the 2nd and 3rd orders in the variables (ψ, w) written in conservative and non-conservative forms, and similar effects were revealed for non-conservative schemes in large scales (not shown in Fig. 2).

For conservative schemes, for example, for CCS there exists a certain time interval for energy transport over the spectrum, and so, starting an experiment, we see that the energy is transported to large scales gradually. However, this is not the case for cubic, Hermite, spline schemes, the energy is transported to the largest scales immediately after start of calculations. The excessive energy transport to large scales may be explained by incorrect description of nonlinear interactions in those schemes. In the case of Hermite scheme, aliasing errors play a considerable role. Removing these errors with the use of a filter for all harmonics with the wave-

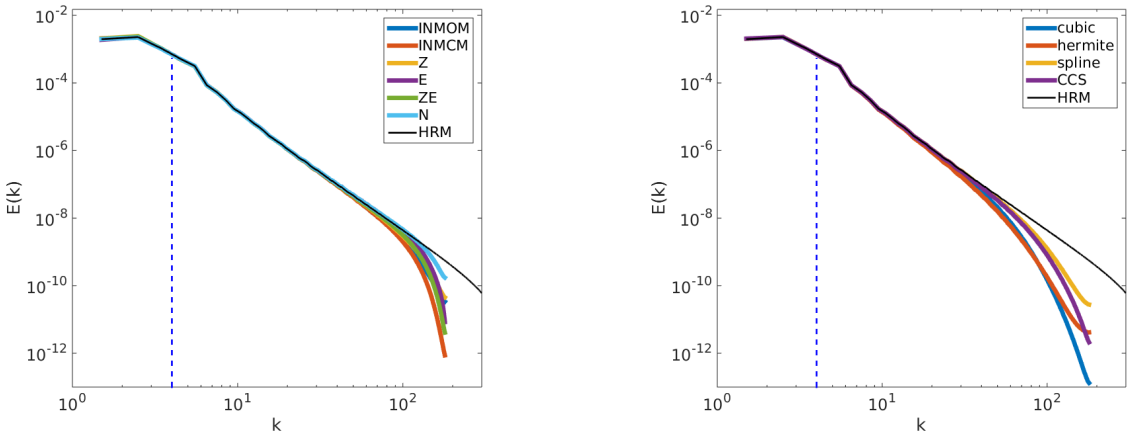

(a) Finite difference schemes.

(b) Semi-Lagrangian schemes, variables (ψ, w).

Figure 3. Energy spectrum in the logarithmic scale in the experiment with large-scale forcing, dotted line denotes the position of forcing.

length lesser than $4h$ [19], one can change energetic properties of the scheme (energy generation is replaced by dissipation in the scheme), but the accumulation of energy at large scales remains.

4.2 Large-scale forcing

The resolution of the computational grid was taken equal to 360×360 points. The forcing was near the wave number $k_f = 4$ with the thickness of the circular shell in the spectral space equal to $k_\delta = 4$. The energy influx ε and the coefficient α of Rayleigh friction were taken the same as in the experiment with small-scale forcing. The coefficient at the biharmonic operator was taken equal to $\nu = 1.06 \cdot 10^{-9}$ and was obtained from formula (2.17). The equations were solved until the statistical equilibrium at t = 1000 and then the calculations were continued for 80000 time units to obtain averaged values with high accuracy. The calculations on the grid of 1008×1008 nodes were taken as the reference HRM solution.

Figure 3 shows the spectral energy distributions for the studied schemes. The figure presents only semi-Lagrangian methods in the variables (ψ, w). The large-scale part of the spectrum is the same for all schemes; the small-scale part has an underestimated energy level for difference schemes up to waves of $6h$, and for semi-Lagrangian schemes up to $12\,h$. It is interesting that the N scheme which do not posses invariants in the asymptotics $F = D = 0$ lies most close to the spectrum of the reference HRM solution.

The energy level differs from scheme to scheme by less than 1%. In the introduction we have indicated the possibility to transport errors over the spectrum into large scales and also the presence of aliasing errors. We can conclude that even with the resolution of 360×360 they cannot change the equilibrium state.

5 Conclusions

In the present paper we studied the influence of the method of discretization of advective terms in equations of two-dimensional incompressible fluid on the statistically equilibrium distribution of energy over the spectrum. The choice of schemes was first of all motivated by the development strategy of the climate model developed in the INM RAS. The central problem of our study was a quantitative answer to the question on the necessity of conservation laws for the enstrophy and energy in the asymptotic case of an ideal fluid in the problem of simulation of a forced two-dimensional turbulence.

The main results of the paper are in the following conclusions.

1. In experiments with small-scale forcing, when the forcing is on the characteristic scale of the computational grid, the role of 'conservation laws' is clearly revealed. The generation of enstrophy can lead to violation of the inverse cascade (INMOM, E) and its dissipation does not always lead to serious consequences (INMCM) because in this case the dissipation begins to replace the numerical filter. Non-conservation of the integral vorticity leads to accumulation of the energy on largest scales (cubic, Hermite, spline). This effect is especially pronounced for the Hermite scheme. In the reproduction of the inverse energy cascade the requirement of energy conservation is irrelevant (INMCM, Z, N, CCS).
2. In experiments with a large-scale forcing when the forcing is well resolved on the grid, the level of the energy spectrum in large and medium scales coincides with the level of the high resolution model, and the differences are observed in small scales only where scheme effects appear and expands up to $6h$ in finite difference schemes and up to $12\,h$ in semi-Lagrangian schemes.

Funding: The work was performed in the INM RAS and supported by the Russian Foundation for Basic Research (project 16–55–12015) and by the Russian Science Foundation (analysis of semi-Lagrangian schemes in Sections 3.3, 3.4, 4) project 14–27–00126.

References

[1] V. Alekseev, E. Volodin, and V. Galin, Simulation of present-day climate with the INM RAS atmospheric model. *Preprint INM RAS No. 215*. Inst. Numer. Math., Moscow, 1998 (in Russian).
[2] K. Alvelius, Random forcing of three-dimensional homogeneous turbulence. *Phys. Fluids* **11** (1999), 1880–1889.
[3] A. Arakawa, Computational design for long-term numerical integration of the equations of fluid motion: Two-dimensional incompressible flow. Part I. *J. Comp. Phys.* **1** (1966), 119–143.
[4] A. Arakawa and V. Lamb, Computational design of the basic dynamical processes of the UCLA general circulation model. *Methods Comp. Phys.* **17** (1977), 173–265.
[5] L. Berselli, T. Iliescu, and W. Layton, *Mathematics of Large Eddy Simulation of Turbulent Flows*. Springer, Scientific Computation, New York, 2005.
[6] G. Boffetta, A. Celani, and M. Vergassola, Inverse energy cascade in two-dimensional turbulence: Deviations from Gaussian behaviour. *Phys. Rev.* **61** (2000), No. 1, R29.
[7] G. Boffetta and S. Musacchio, Evidence for the double cascade scenario in two-dimensional turbulence. *Phys. Rev. E* **82** (2010), No. 1, 016307.
[8] D. Brown, R. Cortez, and M. Minion, Accurate projection methods for the incompressible Navier–Stokes equations. *J. Comp. Phys.* **168** (2001), 464–499.
[9] N. Dianskii, A. Bagno, and V. Zalesny, Sigma model of global ocean circulation and its sensitivity to variations in wind stress. *Izv. Atmos. Ocean. Phys.* **38** (2002), No. 5, 477–494.
[10] V. Dymnikov, *Stability and Predictability of Large-Scale Atmospheric Processes*. INM RAS, Moscow, 2007 (in Russian).
[11] M. Hortal, The development and testing of a new two-time-level semi-Lagrangian scheme (SETTLS) in the ECMWF forecast model. *Quart. J. Royal Meteorol. Soc.* **128** (2002), 1671–1687.
[12] R. Kraichnan, Inertial ranges in two-dimensional turbulence. *Phys. Fluids* **10** (1967), 1417–1423.
[13] D. Lilly, The representation of small scale turbulence in numerical simulation experiments. In: *Proc. of IBM Scientific Computing Symp. Environ. Sci.* 1967, pp. 195–210.
[14] A. McDonald, Accuracy of multiply-upstream, semi-Lagrangian advective schemes. *Month. Weather Rev.* **112** (1984), 1267–1275.
[15] Y. Morinishi, T. Lund, O. Vasilyev, and P. Moin, Fully conservative higher order finite difference schemes for incompressible flow. *J. Comp. Phys.* **143** (1998), 90–124.
[16] R. Nair, J. Scroggs, and F. Semazzi, Efficient conservative global transport schemes for climate and atmospheric chemistry models. *Month. Weather Rev.* **130** (2002), 2059–2073.
[17] T. Palmer, Towards the probabilistic Earth-system simulator: a vision for the future of climate and weather prediction. *Quart. J. Royal Meteorol. Soc.* **138** (2012), 841–861.
[18] C. Pasquero and G. Falkovich, Stationary spectrum of vorticity cascade in two-dimensional turbulence. *Phys. Rev. E* **65** (2002), No. 5, 056305.
[19] N. Phillips, An example of non-linear computational instability. In: *Atmosphere and the Sea in Motion*. Rockefeller Institute Press, New York, 1959, pp. 501–504.
[20] R. Purser and L. Leslie, An efficient interpolation procedure for high-order three-dimensional semi-Lagrangian models. *Month. Weather Rev.*, **119** (1991), 2492–2498.

[21] R. Salmon, *Lectures on Geophysical Fluid Dynamics*. Oxford Univ. Press, New York, 1998.
[22] V. Shashkin, R. Fadeev, and M. Tolstykh, 3D conservative cascade semi-Lagrangian transport scheme using reduced latitude–longitude grid (CCS-RG). *J. Comp. Phys.* **305** (2016), 700–721.
[23] A. Staniforth and J. Côté, Semi-Lagrangian integration schemes for atmospheric models-a review. *Month. Weather Rev.* **119** (1991), No. 9, 2206–2223.
[24] M. Tolstykh, *Global Semi-Lagrangian Numerical Weather Prediction Model*. FOP, Obninsk–Moscow, 2010 (in Russian).
[25] C. Tran and J. Bowman, Robustness of the inverse cascade in two-dimensional turbulence. *Phys. Rev. E* **69** (2004), No. 3, 036303.
[26] E. Tyrtyshnikov, *A Brief Introduction to Numerical Analysis*. Birkhäuser, Boston, 1997.
[27] S. Verma and Y. Xuan, An improved bounded semi-Lagrangian scheme for the turbulent transport of passive scalars. *J. Comp. Phys.* **272** (2014), 1–22.
[28] D. Williamson and P. Rasch, Two-dimensional semi-Lagrangian transport with shape-preserving interpolation. *Month. Weather Rev.* **117** (1989), 102–129.
[29] D. Xiu and G. Karniadakis, A semi-Lagrangian high-order method for Navier–Stokes equations. *J. Comp. Phys.* **172** (2001), 658–684.